AGU PUBLICATIONS

Geophysical Research Letters

RESEARCH LETTER
10.1002/2015GL066774

Key Points:
- Effect of air-sea coupling on intense TC distribution was investigated
- In 60 km AOGCM, intense TC distribution becomes more realistic than in AGCM
- Subsurface oceanic condition is important for the intense TC north of 20°N

Supporting Information:
- Supporting Information S1

Correspondence to:
T. Ogata,
ogata.tomomichi.ga@u.tsukuba.ac.jp

Citation:
Ogata, T., R. Mizuta, Y. Adachi, H. Murakami, and T. Ose (2015), Effect of air-sea coupling on the frequency distribution of intense tropical cyclones over the northwestern Pacific, *Geophys. Res. Lett.*, *42*, 10,415–10,421, doi:10.1002/2015GL066774.

Received 27 OCT 2015
Accepted 21 NOV 2015
Accepted article online 1 DEC 2015
Published online 11 DEC 2015

Effect of air-sea coupling on the frequency distribution of intense tropical cyclones over the northwestern Pacific

Tomomichi Ogata[1], Ryo Mizuta[2], Yukimasa Adachi[2,3], Hiroyuki Murakami[4], and Tomoaki Ose[2]

[1]Faculty of Life and Environmental Sciences, University of Tsukuba, Tsukuba, Japan, [2]Meteorological Research Institute, Tsukuba, Japan, [3]Japan Meteorological Agency, Tokyo, Japan, [4]Geophysical Fluid Dynamics Laboratry, Princeton, New Jersey, USA

Abstract Effect of air-sea coupling on the frequency distribution of intense tropical cyclones (TCs) over the northwestern Pacific (NWP) region is investigated using an atmosphere and ocean coupled general circulation model (AOGCM). Monthly varying flux adjustment enables AOGCM to simulate both subseasonal air-sea interaction and realistic seasonal to interannual sea surface temperature (SST) variability. The maximum of intense TC distribution around 20–30°N in the AGCM shifts equatorward in the AOGCM due to the air-sea coupling. Hence, AOGCM reduces northward intense TC distribution bias seen in AGCM. Over the NWP, AOGCM-simulated SST variability is large around 20–30°N where the warm mixed layer becomes shallower rapidly. Active entrainment from subsurface water over this region causes stronger SST cooling, and hence, TC intensity decreases. These results suggest that air-sea coupling characterized by subsurface oceanic condition causes more realistic distribution of intense TCs over the NWP.

1. Introduction

The northwestern Pacific (NWP) region is the most active region for tropical cyclones (TCs). Surrounding land area, East Asia, has large population, and hence, social and economic loss by TCs is a serious issue. Therefore, accurate future projection of TCs over the NWP is important [e.g. *Yokoi and Takayabu*, 2009; *Knutson et al*., 2010; *Murakami et al*., 2011; *Colbert et al*., 2015]. On the other hand, current climate models still have bias for TC simulation skill over the NWP. Recent advances of computational resources have enabled high-resolution general circulation model (GCM) simulation. For example, using the 20 km resolution atmospheric general circulation model (AGCM) (MRI-AGCM3.2S), *Murakami et al*. [2012a] reported that the simulated intensity of global tropical cyclones was significantly improved, as compared with results of the previous version 20 km resolution AGCM (MRI-AGCM3.1S). However, although TC intensity distribution in MRI-AGCM3.2S becomes comparable to the observation, spatial distribution of intense TCs with maximum wind speed larger than 70 m/s (Category 5 or C5) shifts more northward (around 20–30°N) compared to observation [see *Murakami et al*., 2012a, Figure 12d]. Therefore, more accurate simulation of intense TCs under current climate condition is needed for more reliable future projections.

Some possible causes of such intense TC distribution bias have been studied. One is due to insufficient horizontal resolution of the atmospheric component. *Kanada et al*. [2013] investigated rapid intensification of intense TCs using regional nonhydrostatic atmospheric model. They pointed out that 2 km or finer resolution is needed to simulate realistic rapid intensification, and hence, the lack of such rapid intensification may cause northward bias of intense TC distribution. Another is lack of air-sea coupling process. Sea surface temperature (SST)-prescribed AGCM simulation neglects rapid and large TC-induced SST cooling and subsurface oceanic conditions [e.g. *Price*, 2009; *Vincent et al*., 2012a; *Lloyd and Vecchi*, 2011]. As one of the factors contributing to TC intensification rate and maximum potential intensity, tropical cyclone heat potential (TCHP) has been proposed. TCHP is defined as heat content of water above the 26°C isotherm [e.g. *Leipper and Volgenau*, 1972; *Gray*, 1979; *Wada and Usui*, 2007]. Over the NWP, oceanic mixed layer becomes shallow around 20–30°N by the underlying subtropical mode water (STMW) [e.g. *Oka and Qiu*, 2012] as compared with that around 10–20°N. This fact indicates that in the north of 20°N where mixed layer is shallow, air-sea coupling will suppress the intense-TC intensification through SST cooling. Such air-sea coupling process therefore can be expected to reduce the northward bias seen in SST-prescribed AGCM. To take into account these air-sea coupling processes, coupling with ocean GCM (OGCM) is needed. In this study, we focus on the effect of air-sea coupling on TCs over the NWP region with 60 km resolution atmosphere and ocean-coupled GCM (AOGCM).

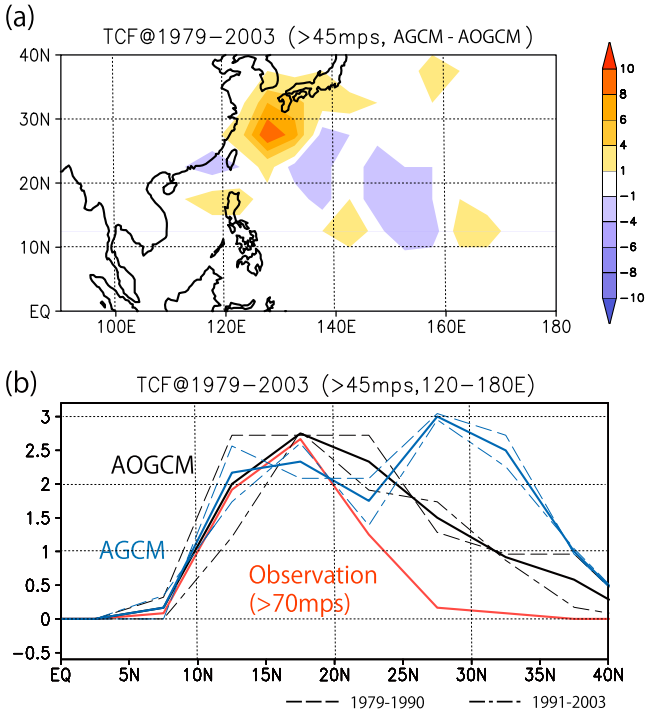

Figure 1. (a) Difference in the intense TC frequency (TCF: maximum wind speed >45 m/s) between the two runs (AGCM run and AOGCM run) in 5° × 5° bins during 1979–2003 (unit numbers/25 yr). (b) Zonal average of intense TCF between 120 and 180°E (in 5° × 5° bins: unit numbers/25 yr). AOGCM (AGCM) runs are black (blue) curves. Solid lines show 25 yr average during 1979–2003, and dashed lines show subsamples of 12 year average (1979–1990) and 13 year average (1991–2003). For comparison, observed extreme TCF (C5: maximum wind speed >70 m/s) is superposed on red curve.

2. Data and Models

In this study, we used AOGCM consisting of an atmospheric component of MRI-AGCM3.2H [*Mizuta et al.*, 2012] with a 60 km horizontal resolution and 64 vertical levels (TL319L64) and an oceanic component of MRI.COM3 [*Tsujino et al.*, 2010] with tripolar grid with 1° zonal and 0.5° meridional resolutions and 50 vertical levels. Using the 20 km resolution version of MRI-AGCM3.2 (MRI-AGCM3.2S), *Murakami et al.* [2012a] reported that the simulated intensity of global tropical cyclones was significantly improved, as compared with results of the previous version (MRI-AGCM3.1S). In 60 km AGCM, for smaller computational cost, multiensemble simulations (different SST pattern, convection schemes) were executed, and their uncertainty for the simulated TC distribution was reported [*Murakami et al.*, 2012b].

To achieve a realistic model simulation in a coupled GCM, flux adjustment is often used [*Yukimoto et al.*, 2006]. In order to simulate both subseasonal air-sea interaction and realistic seasonal to interannual SST variability, year-to-year monthly varying flux adjustment was applied to AOGCM. First, AOGCM run with strong SST restoring (~1 day) to monthly HadISST was executed to obtain the necessary surface flux. Then, AOGCM run without SST restoring but with the obtained monthly flux adjustment was executed. Using AOGCM-simulated monthly mean SST, we also executed SST-prescribed AGCM run to investigate the air-sea coupling effect with same SST boundary condition. SST update interval is 3600 s in AOGCM and 86,400 s in AGCM. Here we refer SST-prescribed run (MRI-AGCM3.2H with AOGCM SST) as "AGCM run" while air-sea coupled run (MRI-AGCM3.2H with the ocean model of MRI.COM3) as "AOGCM run". Both runs were integrated from January 1979 to December 2003.

3. Results

First, we investigate the air-sea coupling effect on the climatological TC statistics between AGCM and AOGCM runs. Figure 1a shows TC-frequency (TCF) difference between these two runs in 5° × 5° bins during 1979–2003 (see *Murakami et al.* [2012a] for details of TC tracking method). Only TCs stronger than C3 (maximum wind speed > 45 m/s) are chosen. Different from previous study using 20 km AGCM [*Murakami et al.*, 2012a], we choose lower C3 criteria because C4 and C5 extreme TCs are rarely seen in 60 km AGCM. Although 60 km AGCM has a bias in TC intensity distribution due to coarse resolution "quantitatively", 20 km and 60 km AGCM shares a similarity in northward TC intensity peak bias [*Murakami et al.*, 2012b]. This study mainly focuses on whether air-sea coupling process can reduce the northward bias "qualitatively" by comparing 60 km AGCM and AOGCM simulations. Positive TCF difference around (20–30°N, 120–130°E) means that the AGCM run tends to simulate intense TCs more frequently than the AOGCM run. This implies that the air-sea coupling in AOGCM is an important factor for intense TCF. Figure 1b shows the meridional distribution of zonal averaged (from 120°E to 180°E) intense TCF during 1979–2003. In AOGCM run (black lines), intense TCF peak locates around 15–25°N, while AGCM run (blue lines) has another peak around 30°N. Similar TCF

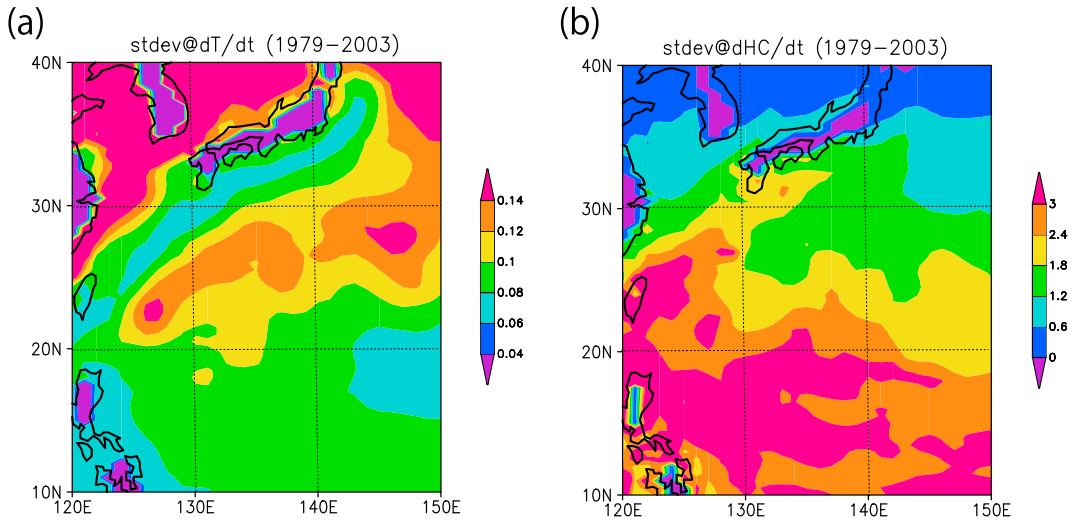

Figure 2. Standard deviation of time tendency of (a) SST (unit °C/d), and (b) TCHP (unit °Cm/d) during June–November simulated in the AOGCM run. To focus on subseasonal variability, 31 day high-pass filter was applied.

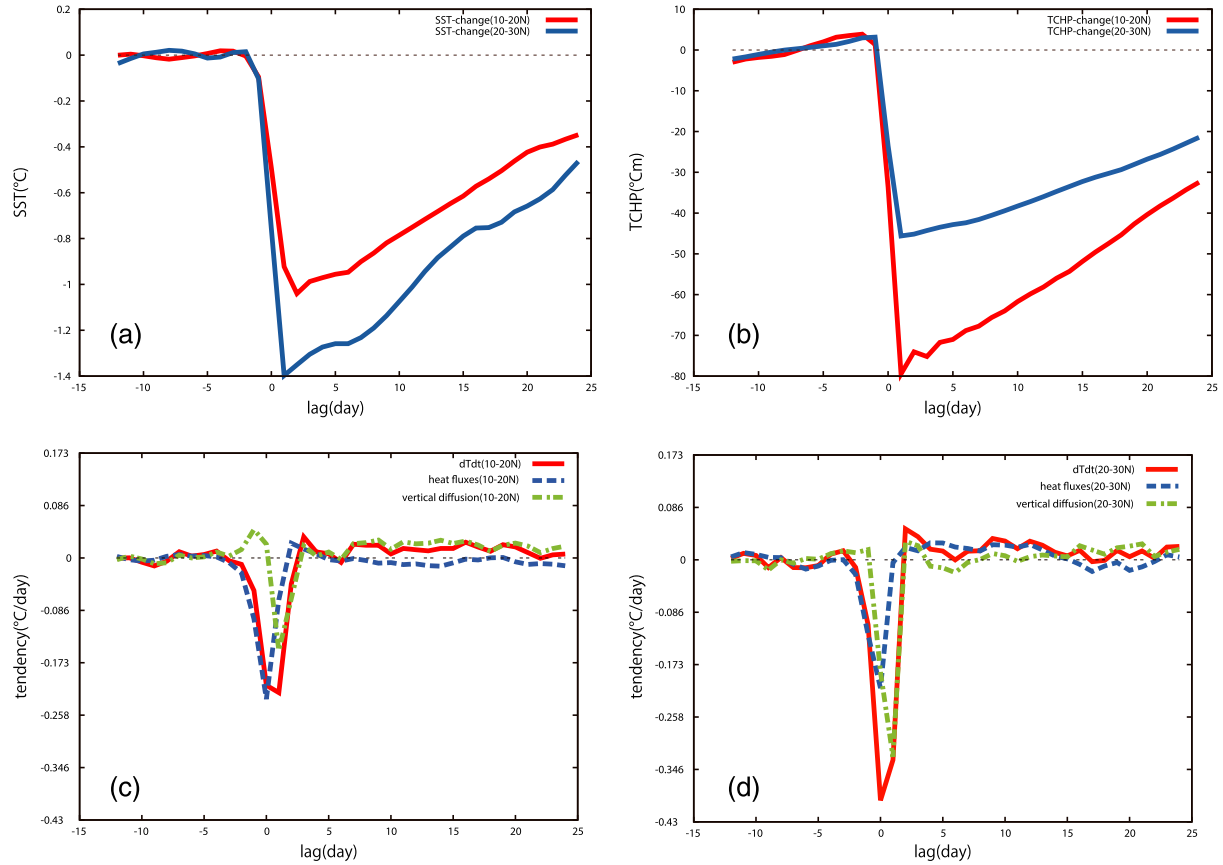

Figure 3. (a) Composite SST (unit °C) variability along the TC tracking. (b) Same as Figure 3a but for TCHP (unit °Cm). In Figures 3a and 3b, 10–20°N (20–30°N) is drawn by red (blue) lines. To emphasize the cooling, relative anomalies from −12 to −2 day average are shown. (c) Heat budget over the ML along the TC tracking on 10–20°N. (d) Same as Figure 3c but for 20–30°N. In Figures 3a–3d, day 0 is defined when intense TCs are passing at the certain location and negative (positive) lags mean before (after) the TCs passage there.

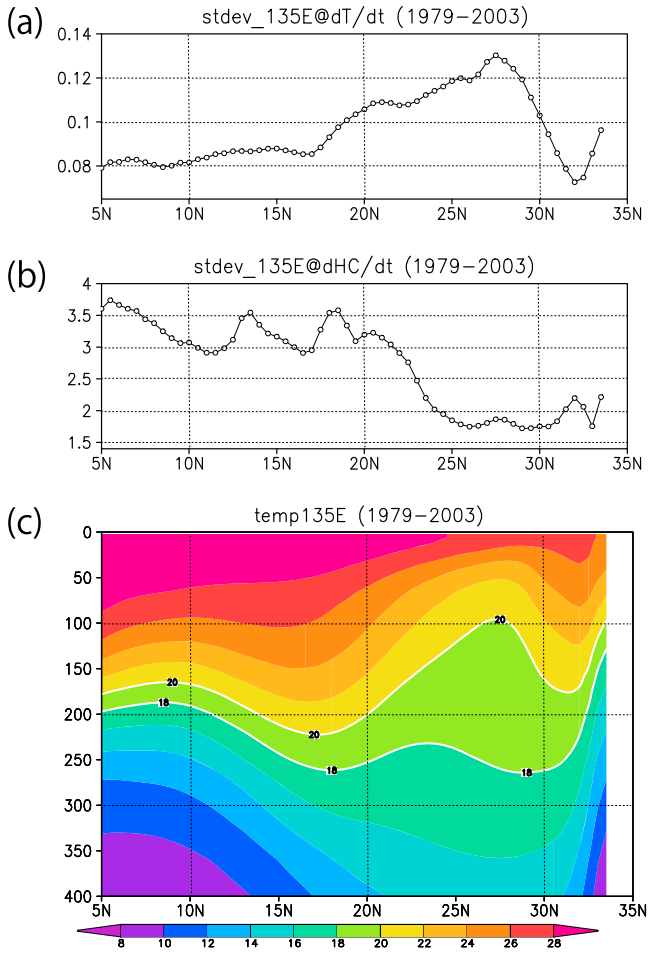

Figure 4. Standard deviations of time tendency of (a) SST (unit °C/d), and (b) TCHP (unit °Cm/d) during June–November at 135°E. (c) Climatological upper ocean temperature (unit °C) during June–November at 135°E in the AOGCM run. To focus on the thick subtropical mode water (STMW) in Figure 4c, 18°C and 20°C isotherms are emphasized by white contours.

shapes in different periods (dashed lines in Figure 1b: 1979–1990 and 1991–2003) support that intense TCF in AGCM run is robustly larger around 25–35°N than in AOGCM run. It should be noted that mean TC intensity generally decreases in AOGCM run compared to AGCM run (see supporting information).

As mentioned in section 1, spatial distribution of 20 km AGCM-simulated extreme TCs with maximum wind speed more than 70 m/s (Category 5 or C5) is located more northward (around 20–30°N) compared to observation [see *Murakami et al.*, 2012a, Figure 12d]. Joint Typhoon Warning Center has provided best track data since 1945 over the NWP (http://weather.unisys.com/hurricane/). For comparison, observed extreme TCF during 1979–2003 is superposed on red line in Figure 1b. Observed extreme TCF peak is located around 10–20°N, and such TCF rapidly decays north of 20°N. In the observed extreme TCF, compared to the intense TCF in the AOGCM run, larger SST cooling (cold wake) by stronger TC-induced mixing may cause the rapid decay of the TCF distribution. TCF in the AOGCM run shows more realistic features (e.g. peak around 10–20°N, disappearance of another peak around 30°N) than in the AGCM run. These results imply that air-sea coupling featured by subsurface oceanic condition causes more realistic intense TC distribution over the NWP.

The subseasonal oceanic response (SST and TCHP) over the NWP is shown in Figure 2. Figure 2a shows standard deviation of time tendency of the SST (dT/dt) from June to November in the AOGCM run, which is a measure of subseasonal SST change. Over the NWP, large SST change appears south of Japan (around 20–30°N), which corresponds to the TC decaying region. Such SST change implies that rapid SST cooling hampers TC intensification. The SST change is small south of 20°N and southern coast of Japan, where oceanic mixed layer is deep, and hence, SST is less sensitive to the atmospheric heat fluxes and vertical mixing. Furthermore, Figure 2b shows standard deviation of time tendency of TCHP. Large TCHP change appears south of 20°N which corresponds to the TC growing region. This region is a part of warm pool region with deep warm water (>26°C) in approximately upper about 100 m. In contrast, rapid decrease of TCHP change north of 20°N is due to rapid shoaling of warm water thickness (in the upper about 50 m or less). It should be also noted that in the north of 20°N, maximum of TCHP change extends along the Kuroshio path (as the western boundary current over the NWP). This implies that warm water advection along the Kuroshio path maintains warm water volume.

To emphasize the cooling induced by intense TCs, Figure 3a shows composite SST variability along the TC tracking [e.g. *Lloyd and Vecchi*, 2011; *Jullien et al.*, 2014]. Time series of SST variability at the fixed location are composited for all the positions where the intense TCs pass over. Day 0 is defined when the TC is passing over the position. South of 20°N (162 samples), maximum SST cooling induced by intense TCs is about −1°C at day +2, while it is about −1.4 °C at day +1 north of 20°N (108 samples) (Figure 3a). Stronger cooling north of 20°N can be explained by ocean stratification; TCHP before TC passage (Day −12 to Day −2) is

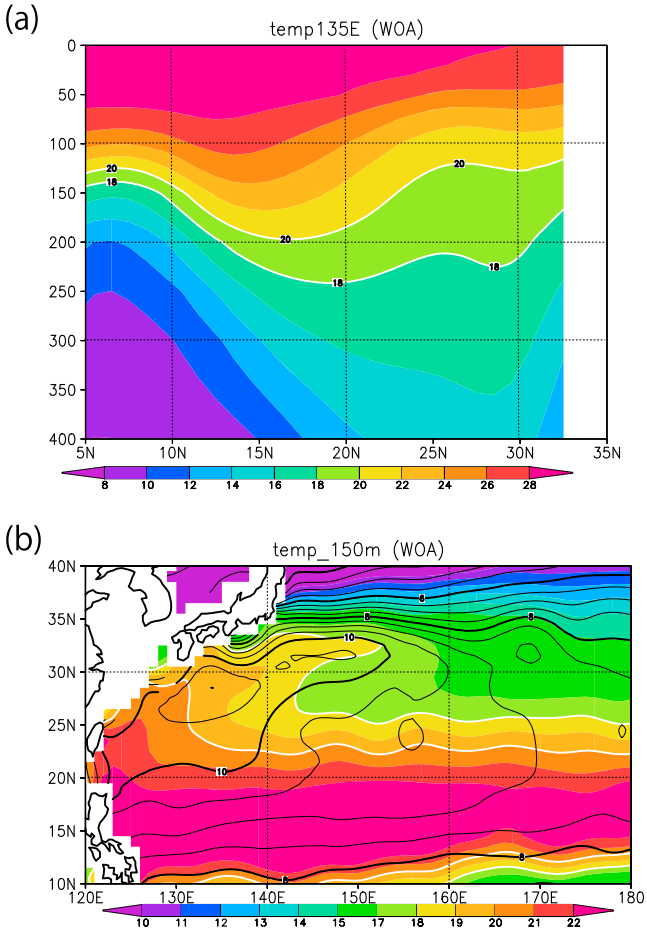

Figure 5. (a) Similar to Figure 4c but for observation [*Boyer et al.*, 1998]. (b) Observed temperature at 150 m depth (shaded and white contours) and vertical averaged temperature between 150 and 1000 m depth (black contours, as a measurement of stream function). 18°C and 20°C isotherms are emphasized by white contours.

indeed stronger south (146.2°Cm) than north (71.3°Cm) of 20°N (not shown). Such TCHP difference prior to TC passage implies that more energy is required in the south to mix water colder than 26°C into the surface layer. Regarding the TCHP response to TCs, we find a weaker anomaly in the north (−50°Cm at Day +1) than in the south (−80°Cm at Day +1) (Figure 3b). Such smaller TCHP anomaly despite larger SST cooling north of 20°N is consistent with the result of Figure 2. A reason for this might be that weak TCHP prior to TC passage cannot undergo a very strong anomaly (e.g., an initial TCHP of 71.3°Cm in the north cannot undergo an anomaly of −80 Cm as occurs in the south). It should also be noted that TCHP is not a perfect index to account for the oceanic control of TC-induced cooling [e.g. *Price*, 2009; *Vincent et al.*, 2012a].

Why the peak of the subseasonal SST change (Figure 2) is located around 20–30°N? Figures 3c and 3d show heat budget analysis over the mixed layer (ML) (ML depth is defined by SST-0.5°C) along the TC tracking. North of 20°N, larger ML temperature cooling (red lines; 1.7 times larger than south of 20°N) is mainly due to the oceanic terms by advection and diffusion (green lines; 2 times larger than south of 20°N). On the other hand, surface heat flux is comparable between north and south of 20°N (blue lines). This implies that ocean dynamics (e.g., vertical mixing and cold advection by Ekman pumping) is important for larger SST cooling north of 20°N. Some previous studies have pointed out the importance of ocean dynamics for TC induced SST cooling [e.g., *Vincent et al.*, 2012b; *Jullien et al.*, 2014]. For example, using OGCM simulation, *Vincent et al.* [2012b] showed that vertical mixing is much more effective over the shallow ML and sharp temperature stratification than deep ML. Our study further suggests the impact on the TC distribution (Figure 1).

Figure 4 shows subseasonal SST and TCHP changes and mean temperature above 400 m depth along 135°E. In mean temperature (Figure 4c), there is thick subsurface (18–20°C) water, and it pushes up the thermocline up to 50 m depth. Such cold subsurface water is known as "subtropical mode water" (STMW) [e.g. *Oka and Qiu*, 2012], which is formed over the Kuroshio extension region where warm water loses buoyancy due to the atmospheric cooling and generates deep uniform water mass. The water mass subducts below the thermocline and moves to southwestward (around 20–30°N). Such thick subsurface water appears in observation (Figure 5a) although structure is diffused. From Figure 5b, such subsurface cold water can be traced back to the Kuroshio extension region around 35°N, 150°E along the southwestward flow. As a result, such shallow mixed layer and thick subsurface cold water seem to play a key role for large subseasonal SST change in response to the atmospheric forcing through active entrainment of subsurface water (Figure 4a). On the other hand, TCHP change is rapidly decreasing north of 20°N (Figure 4b) because the volume of warm water (>26°C) is also rapidly decreasing at the same location.

4. Summary and Discussion

Effect of air-sea coupling on the frequency distribution of tropical cyclones (TCs) over the northwestern Pacific (NWP) region is investigated using 60 km resolution atmosphere and ocean coupled general circulation model (AOGCM). In AOGCM, oceanic response to TC forcing shows SST and subsurface temperature cooling after TC passage. In AOGCM, maximum of intense TC distribution is located around 15–25°N, while peak around 30°N seen in SST-prescribed AGCM disappears due to the air-sea coupling. Over the NWP, simulated SST variability is large around 20–30°N where the warm mixed layer becomes shallower rapidly with latitudes. Active entrainment over this region causes stronger SST cooling, and hence, TC intensity becomes weak. On the other hand, AOGCM simulated TC heat potential (TCHP) variability is large south of 20°N. South (north) of 20°N, large (small) TCHP with deep (shallow) warm water volumes over 26°C causes large (small) TCHP variability, which causes large (small) heat conversion rate from warm ocean to TC. These results suggest that air-sea coupling featured by subsurface oceanic condition causes more realistic intense TC distribution over the NWP.

More recently, *Murakami et al*. [2015] investigated TC activity in GFDL coupled GCM (HiFLOR). HiFLOR (25 km resolution AGCM) simulates extreme intense TCs (C4 and C5) better than FLOR (50 km resolution AGCM). Their study suggests that finer resolution AOGCM simulation is a key factor for realistic extreme intense TCs distribution. On the other hand, previous studies have pointed out that different AGCM components (i.e., intermodel comparison among different convection schemes) give quantitative and qualitative uncertainties for climatological total or intense TC distribution and its future change. As a next step, 20 km resolution AOGCM experiment is necessary to more accurate estimation of air-sea coupling under more realistic TC intensity. Furthermore, STMW (18–20°C water in Figure 4c) in AOGCM is too clear compared to diffused profile in observations (Figure 5a), which suggests that high-resolution ocean (20 km or finer to capture the oceanic mesoscale eddies and narrow coastal currents) [e.g. *Masumoto et al*., 2004; *Hayasaki et al*., 2013; *Ogata and Kitoh*, 2014] may be also important to capture more adequate TC life cycle. Previous studies suggest that the high-resolution ocean may affect TC-induced upwelling [*Vincent et al*., 2012b, Figure 2] and modulate SST cooling by mesoscale eddies [*Jullien et al*., 2014, Figure 13]. Our study focused on air-sea coupling effect in 60 km resolution AOGCM, but these results imply that further investigation of resolution sensitivity (further experiments with 20 km resolution AOGCM) and intermodel comparison between these AOGCMs will be needed.

Acknowledgments
The model data used in this study are available after our consent. If the data are needed, please contact the corresponding author (ogata.tomomichi.ga@u.tsukuba.ac.jp). This work was conducted under the SOUSEI Program of the Ministry of Education, Culture, Sports, Science, and Technology (MEXT) of Japan.

References

Boyer, T. P., S. Levitus, J. I. Antonov, M. E. Conkright, T. O'Brien, C. Stephens, and B. Trotsenko (1998), World Ocean Atlas 1998, vol. 6, Salinity of the Indian Ocean, NOAA Atlas NESDIS, vol. 32, 166 pp., NOAA, Silver Spring, Md.

Colbert, A. J., B. J. Soden, and B. P. Kirtman (2015), The impact of natural and anthropogenic climate change on western North Pacific tropical cyclone tracks, *J. Clim.*, *28*, 1806–1823.

Gray, W. M. (1979), Tropical cyclone intensity determination through upper- troposphere aircraft reconnaissance, *Bull. Am. Meteorol. Soc.*, *60*, 1069–1074.

Hayasaki, M., R. Kawamura, M. Mori, and M. Watanabe (2013), Response of extratropical cyclone activity to the Kuroshio large meander in northern winter, *Geophys. Res. Lett.*, *40*, 2851–2855, doi:10.1002/grl.50546.

Jullien, S., P. Marchesiello, C. E. Menkes, J. Lefèvre, N. C. Jourdain, G. Samson, and M. Lengaigne (2014), Ocean feedback to tropical cyclones: Climatology and processes, *Clim. Dyn.*, *43*(9–10), 2831–2854.

Kanada, S., A. Wada, and M. Sugi (2013), Future changes in structures of extremely intense tropical cyclones using a 2-km mesh nonhydrostatic model, *J. Clim.*, *26*, 9986–10,005.

Knutson, T. R., J. L. McBride, J. Chan, K. Emanuel, G. Holland, C. Landsea, I. Held, J. P. Kossin, A. K. Srivastava, and M. Sugi (2010), Tropical cyclones and climate change, *Nat. Geosci.*, *3*, 157–163.

Leipper, D., and D. Volgenau (1972), Hurricane heat potential of the Gulf of Mexico, *J. Phys. Oceanogr.*, *2*, 218–224.

Lloyd, I. D., and G. A. Vecchi (2011), Observational evidence for oceanic controls on hurricane intensity, *J. Clim.*, *24*, 1138–1153.

Masumoto, Y., et al. (2004), A fifty-year eddy-resolving simulation of the world ocean—Preliminary outcomes of OFES (OGCM for the Earth simulator), *J. Earth Simul.*, *1*, 35–56.

Mizuta, R., et al. (2012), Climate simulations using the improved MRI-AGCM with 20-km grid, *J. Meteorol. Soc. Jpn.*, *90A*, 233–258.

Murakami, H., B. Wang, and A. Kitoh (2011), Future change of western North Pacific typhoons: Projections by a 20-km-mesh global atmospheric model, *J. Clim.*, *24*, 1154–1169.

Murakami, H., et al. (2012a), Future changes in tropical cyclone activity projected by the new high-resolution MRI-AGCM, *J. Clim.*, *25*, 3237–3260.

Murakami, H., R. Mizuta, and E. Shindo (2012b), Future changes in tropical cyclone activity projected by multi-physics and multi-SST ensemble experiments using the 60-km-mesh MRI-AGCM, *Clim. Dyn.*, *39*, 2569–2584.

Murakami, H., et al. (2015), Simulation and prediction of Category 4 and 5 hurricanes in the high-resolution GFDL HiFLOR coupled climate model, *J. Clim.*, doi:10.1175/JCLI-D-15-0216.1.

Ogata, T., and A. Kitoh (2014), Effect of high-resolution SST on 60 km-AGCM simulated snowfall in Japan, *SOLA*, *10*, 131–135, doi:10.2151/sola.2014-027.

Oka, E., and B. Qiu (2012), Progress of North Pacific mode water research in the past decade, *J. Oceanogr.*, *68*, 5–20.
Price, J. F. (2009), Metrics of hurricane-ocean interaction: vertically-integrated or vertically-averaged ocean temperature?, *Ocean Sci.*, *5*, 351–368.
Tsujino, H., T. Motoi, I. Ishikawa, M. Hirabara, H. Nakano, G. Yamanaka, T. Yasuda, and H. Ishizaki (2010), Reference manual for the Meteorological Research Institute Community Ocean Model (MRI.COM) Version 3, *Tech. Rep. of MRI*, 59, 241 pp.
Vincent, E. M., M. Lengaigne, J. Vialard, G. Madec, N. C. Jourdain, and S. Masson (2012a), Assessing the oceanic control on the amplitude of sea surface cooling induced by tropical cyclones, *J. Geophys. Res.*, *117*, C05023, doi:10.1029/2011JC007705.
Vincent, E. M., M. Lengaigne, G. Madec, J. Vialard, G. Samson, N. C. Jourdain, C. E. Menkes, and S. Jullien (2012b), Processes setting the characteristics of sea surface cooling induced by tropical cyclones, *J. Geophys. Res.*, *117*, C02020, doi:10.1029/2011JC007396.
Wada, A., and N. Usui (2007), Importance of tropical cyclone heat potential for tropical cyclone intensity and intensification in the western North Pacific, *J. Oceanogr.*, *63*, 427–447.
Yokoi, S., and Y. N. Takayabu (2009), Multi-model projection of global warming impact on tropical cyclone genesis frequency over the western North Pacific, *J. Meteorol. Soc. Jpn.*, *87*, 525–538.
Yukimoto, S., A. Noda, A. Kitoh, M. Hosaka, H. Yoshimura, T. Uchiyama, K. Shibata, O. Arakawa, and S. Kusunoki (2006), Present-day climate and climate sensitivity in the Meteorological Research Institute coupled GCM Version 2.3 (MRI-CGCM2.3), *J. Meteorol. Soc. Jpn.*, *84*, 333–363.